Incorporating fault zone head wave and direct wave secondary arrival times into seismic tomography: Application at Parkfield, California

Ninfa L. Bennington,[1] Clifford Thurber,[1] Zhigang Peng,[2] Haijiang Zhang,[3] and Peng Zhao[4]

Received 31 May 2012; revised 30 August 2012; accepted 27 December 2012.

[1] We present a three-dimensional (3D) P wave velocity (Vp) model of the Parkfield region that utilizes existing P wave arrival time data, including fault zone head waves (FZHWs), and data from direct wave secondary arrivals (DWSAs). The first-arrival and DWSA travel times are obtained as the global- and local-minimum travel time paths, respectively. The inclusion of FZHWs and DWSAs results in as much as a 5% and a 10% increase in the across-fault velocity contrast, respectively, for the Vp model at Parkfield relative to that of *Thurber et al*. [2006]. Viewed along strike, three pronounced velocity contrast regions are observed: a pair of strong positive velocity contrasts (SW fast), one NW of the 1966 Parkfield earthquake hypocenter and the other SE of the 2004 Parkfield earthquake hypocenter, and a strong negative velocity contrast (NE fast) between the two hypocenters. The negative velocity contrast partially to entirely encompasses peak coseismic slip estimated in several slip models for the 2004 earthquake, suggesting that the negative velocity contrast played a part in defining the rupture patch of the 2004 Parkfield earthquake. Following *Ampuero and Ben-Zion* (2008), the pattern of velocity contrasts is consistent with the observed bilateral rupture propagation for the 2004 Parkfield earthquake. Although the velocity contrasts also suggest bilateral rupture propagation for the 1966 Parkfield earthquake, the fault is creeping to the NW here, i.e., exhibiting velocity-strengthening behavior. Thus, it is not surprising that rupture propagated only SE during this event.

Citation: Bennington, N. L., C. Thurber, Z. Peng, H. Zhang, and P. Zhao (2013), Incorporating fault zone head wave and direct wave secondary arrival times into seismic tomography: Application at Parkfield, California, *J. Geophys. Res. Solid Earth*, *118*, doi: 10.1002/jgrb.50072.

1. Introduction

[2] Large crustal faults such as the San Andreas fault (SAF) typically juxtapose rocks of significantly different elastic properties, resulting in a well-defined across-fault material contrast. As shown in Figure 1, a sharp material contrast across the fault interface is expected to generate fault zone head waves (FZHWs) that spend a large portion of their propagation paths refracting along the interface [*Ben-Zion*, 1989, 1990; *Ben-Zion and Aki*, 1990]. The FZHWs propagate with the velocity of the faster block and are radiated from the fault to the slower velocity block where they are characterized by an emergent waveform with opposite first-motion polarity to that of the direct body waves. Since FZHWs spend most of their propagation paths along the fault interface, they provide a high-resolution tool for imaging the velocity contrast across the major crustal faults [*Ben-Zion and Malin*, 1991; *Ben-Zion et al*., 1992; *McGuire and Ben-Zion*, 2005; *Lewis et al*., 2007; *Zhao and Peng*, 2008; *Zhao et al*., 2010; *Bulut et al*., 2012].

[3] *Zhao et al*. [2010] systematically analyzed large data sets of near-fault waveforms recorded by several permanent and temporary seismic networks along the Parkfield section of the SAF. They found clear FZHWs at many stations on the NE side of the SAF near the San Andreas Fault Observatory at Depth (SAFOD), indicating the presence of a sharp across-fault material contrast in that region. Based on the systematic moveout between the FZHW and associated direct wave secondary arrivals (DWSAs), they estimated an average P wave velocity (Vp) contrast of about 5–10%. In comparison, the FZHW is not clearly developed along the SAF near Gold Hill (GH), located near the 2004 Parkfield earthquake epicenter, and the average Vp contrast is estimated to be 0–2%. The weak evidence for FZHWs and the negligible velocity contrast near GH are consistent

All Supporting Information may be found in the online version of this article.

[1]Department of Geoscience, University of Wisconsin-Madison, Madison, Wisconsin, USA.
[2]School of Earth and Atmospheric Sciences, Georgia Institute of Technology, Atlanta, Georgia, USA.
[3]School of Earth and Space Sciences, University of Science and Technology of China, Hefei, China.
[4]NORSAR, Kjeller, Norway.

Corresponding author: N. L. Bennington, University of Wisconsin-Madison, 1215 W Dayton St., Madison, WI 53706, USA. (ninfa@geology.wisc.edu)

2169-9313/13/10.1002/jgrb.50072

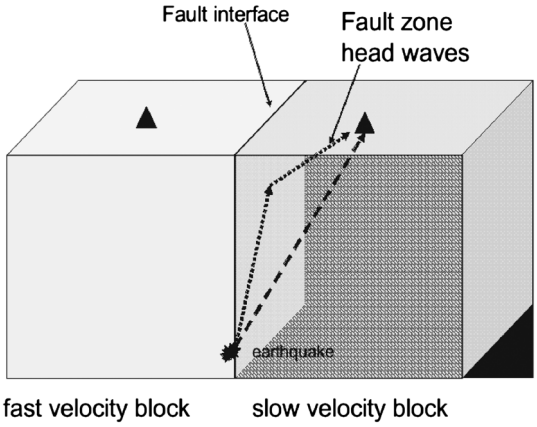

Figure 1. A cartoon demonstrating the FZHW and DWSA propagation paths.

with geophysical observations and geological interpretations of a sliver of high-velocity rock immediately to the NE of the SAF there [*McLaughlin et al*., 1996] and existing three-dimensional (3D) seismic tomography results [*Eberhart-Phillips and Michael*, 1993; *Thurber et al*., 2006]. This is also consistent with a recent study of statistically preferred southeast rupture propagation for microearthquakes in this region [*Lengline and Got*, 2011], suggesting that across-fault material contrast could provide an important control on the earthquake rupture propagation direction [*Andrews and Ben-Zion*, 1997; *Ampuero and Ben-Zion*, 2008].

[4] The local-scale tomography study of *Zhang et al*. [2009] for a roughly 10 km^3 volume centered on SAFOD and the more regional-scale study of *Thurber et al*. [2006] for a 130 km × 120 km × 20 km volume centered on the 1966 Parkfield earthquake rupture provide what are probably the best 3D images of the seismic velocity structure of the area. The former shows a low-velocity zone associated with the SAF extending as deep as 7 km near SAFOD, and both image the well-known velocity contrast across the fault. In this study, we present a model of 3D velocity structure for the Parkfield region that utilizes a combination of existing P wave arrival time data, including FZHWs, plus new data from DWSAs.

[5] The inclusion of FZHWs and DWSAs results in as much as a 5% and a 10% increase in the across-fault velocity contrast, respectively, for the Vp model at Parkfield relative to that of *Thurber et al*. [2006]. In the following sections, we describe in detail how we have included FZHW and DWSA times into a formal inversion for the 3D Vp structure. We discuss the resulting model including comparisons to the Vp model of *Thurber et al*. [2006] and the across-fault velocity contrasts estimated by *Zhao et al*. [2010]. Further comparison is made between the velocity model contrasts determined here and the spatial extent of coseismic slip for the 2004 Parkfield earthquake. Finally, we compare expected rupture propagation directions for the 1966 and 2004 Parkfield earthquakes based on the determined velocity contrasts to the observed rupture propagation directions for the two events.

2. Data Set

[6] Arrival time picks were made manually for earthquakes recorded at Parkfield between 1984 and 2005 on the Parkfield Area Seismic Observatory array, UC-Berkeley High-Resolution Seismic Network, U.S. Geological Survey (USGS) Central California Seismic Network, and USGS temporary stations (Figure 2a). Existing P wave absolute and differential time data as well as cross-correlation data were from *Thurber*

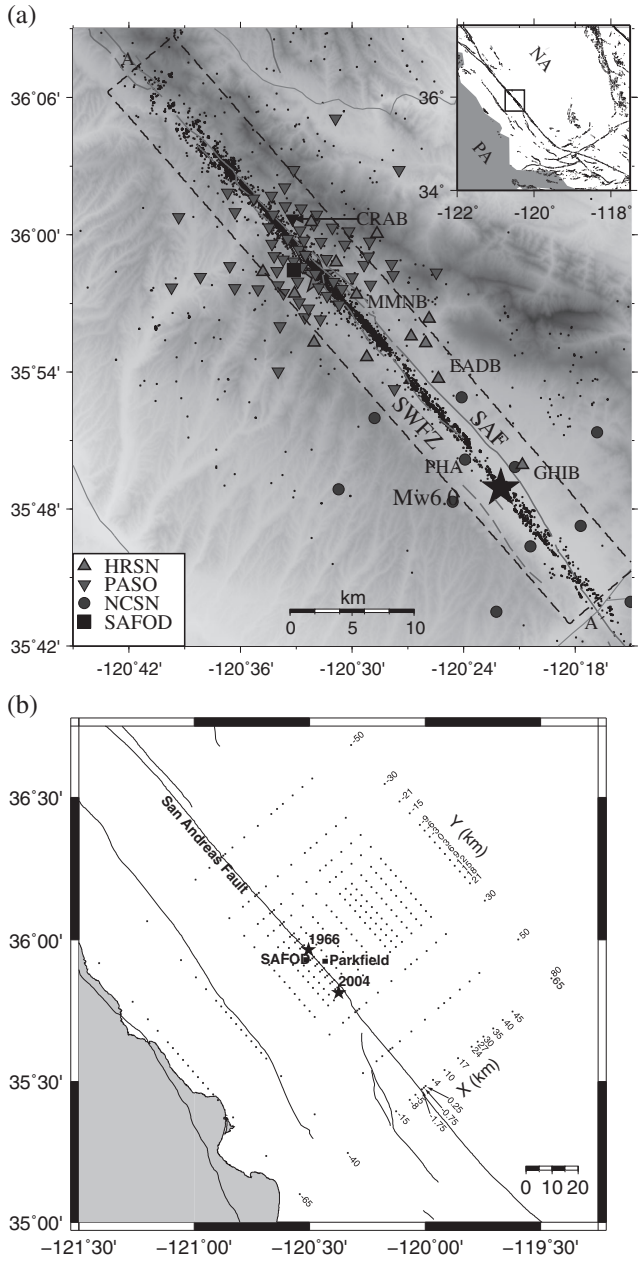

Figure 2. (a) The set of events and stations at Parkfield used in this study. The NW and SE stars indicate the 1966 and 2004 Parkfield earthquakes, respectively. Black dots represent regional seismicity. Figure 1a is adopted from *Zhao et al*. [2010]. (b) Grid used for velocity inversion displayed in map view. Grid nodes are located at X = −65, −40, −15, −8, −5, −1.75, −0.75, 0.25, 4, 10, 17, 24, 27, 30, 35, 40, 45, 65; Y = −70, −50, −30, −21, −18, −15, −12, −9, −6, −3, 0, 3, 6, 9, 15, 21, 30, 50; and Z = 0, 2, 4, 6, 9, 12, 16, 24, 26, and 40 km. The 1966 and 2004 Parkfield earthquakes are indicated as black stars.

et al. [2006] and *Zhang et al*. [2009]. The catalog of FZHW and DWSA picks was from *Zhao et al*. [2010]. DWSA catalog differential times were calculated from this data set.

3. Inversion Details

[7] We have modified the double-difference tomography algorithm tomoDD [*Zhang and Thurber*, 2003] to incorporate FZHW and associated DWSA times into a formal inversion for Vp structure. We have adapted the pseudo-bending method of *Um and Thurber* [1987] to compute travel times for both the first-arriving FZHWs and the later-arriving DWSAs. The pseudo-bending method relies on the fact that for a true ray path satisfying the ray equations, the ray curvature (vector of the second spatial derivative along the path) is everywhere anti-parallel to the component of the velocity gradient normal to the ray path. The pseudo-bending strategy involves locally perturbing an approximate initial ray path (determined from a brute-force search of a "web" of arcuate paths of varying dip and curvature) so that the eikonal equation is satisfied in a piecewise manner and iterating to convergence. The method has proven to be extremely effective when path lengths are up to ~60 km in length, with accuracies comparable to the finite difference method [*Haslinger and Kissling*, 2001]. The strategy for finding secondary arrivals using pseudo-bending is relatively simple. For a DWSA, we force pseudo-bending to derive the direct path instead of the first-arriving FZHW path by modifying tomoDD to restrict the starting path to the vertical plane connecting the earthquake and station and artificially reduce the velocities on the southwest side of the SAF. The pseudo-bending algorithm will thus converge to what is a local-minimum DWSA path instead of the global-minimum FZHW path.

[8] The grid used in this study (Figure 2b) is modified from *Thurber et al*. [2006]. Its nodes at X = −3, −1, and 1 km are repositioned to X = −1.75, −0.75, and 0.25 km so that the relocated nodes fall within and immediately adjacent to along-fault seismicity. Initially, even finer near-fault node spacing was attempted (0.5 km node spacing within 2 km of the fault in the X-direction). However, checkerboard tests (see E-supp Text A and Figure A1 in the Supporting Information) revealed that such fine model parameterization near the fault zone yielded poorly recovered checkers within this region. Thus, the coarser near-fault model parameterization discussed above was used for spacing of nodes in the X-direction.

[9] Since additional data from the local study of *Zhang et al*. [2009] were incorporated, we have created a finer grid near SAFOD by adding nodes at Y = −6, 0, 6, and 12 km. We obtain a starting model by inverting the existing P wave data of *Thurber et al*. [2006] and *Zhang et al*. [2009]. We also include the FZHW times of *Zhao et al*. [2010]. The Vp model of *Thurber et al*. [2006], interpolated onto the modified grid, is used as a starting model. The DWSA times of *Zhao et al*. [2010] are then incorporated into the data set, and the inversion is carried out for the final Vp model.

4. Results and Discussion

[10] The new 3D Vp model for the Parkfield region is presented here in selected fault-normal cross sections (Figures 3a–3f). All cross sections from the inversion are shown in E-supp Figure B1. For the displayed cross sections, top panels represent the starting model, middle panels represent perturbations to the starting model, and bottom panels represent the final Vp model with DWSA times incorporated. We estimate the Vp model quality using a combination of a synthetic recovery test and the derivative weight sum distribution. This parameter reflects the density of rays passing near a grid node where weighting is

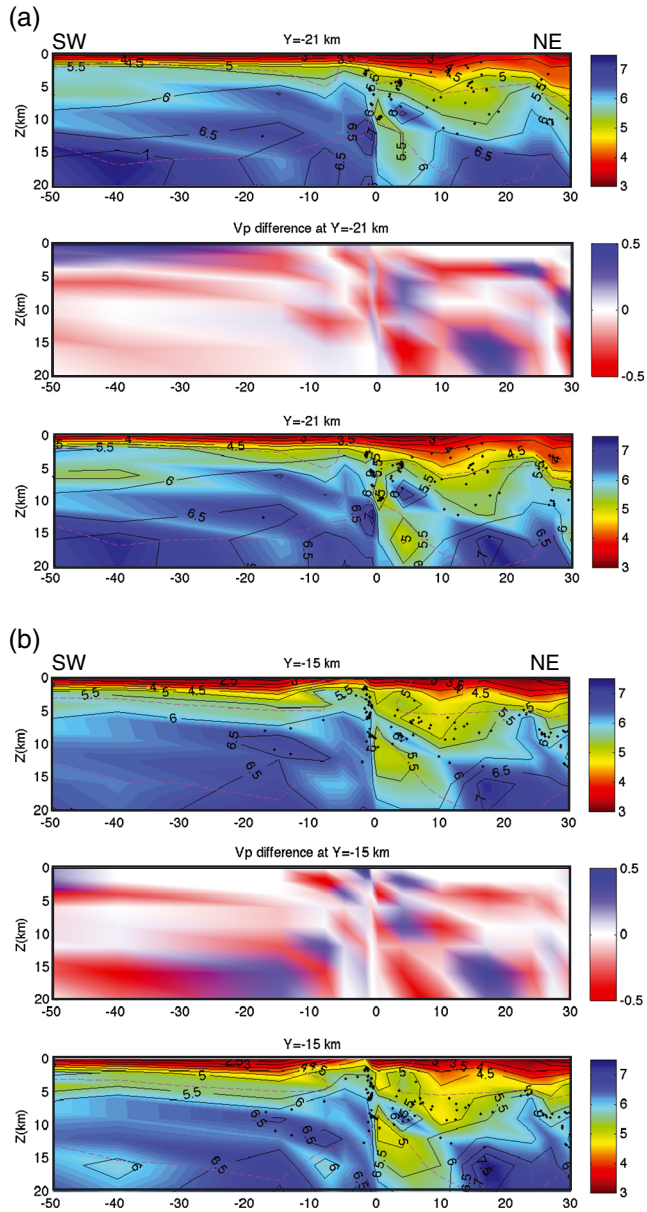

Figure 3. Fault-normal cross sections from Vp inversion at (a) Y = −21, (b) Y = −15, (c) Y = 3, (d) Y = 6, (e) Y = 21, and (f) Y = 30 km. Dashed lines represent well-resolved regions of the model (derivative weight sum values > 200). Black dots represent earthquake hypocenters used in velocity inversion. For displayed Y cross sections, top panels are the starting model, middle panels represent perturbations to the starting model, and bottom panels represent the final velocity inversion results with DWSA times incorporated. Vp is shown in km/s.

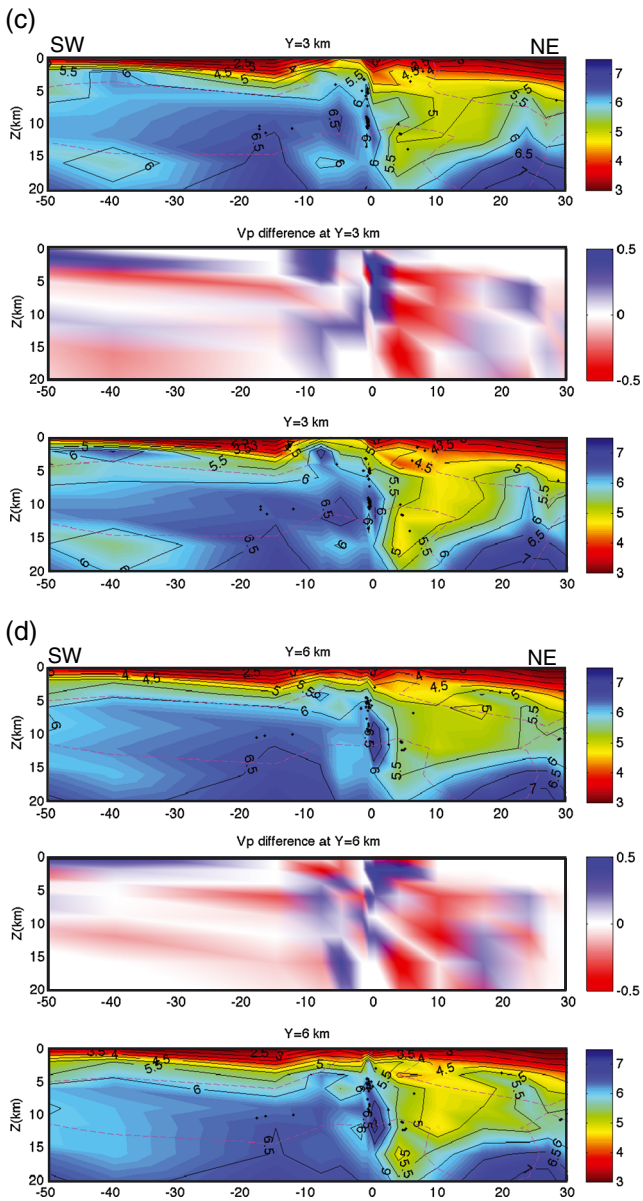

Figure 3. (Continued).

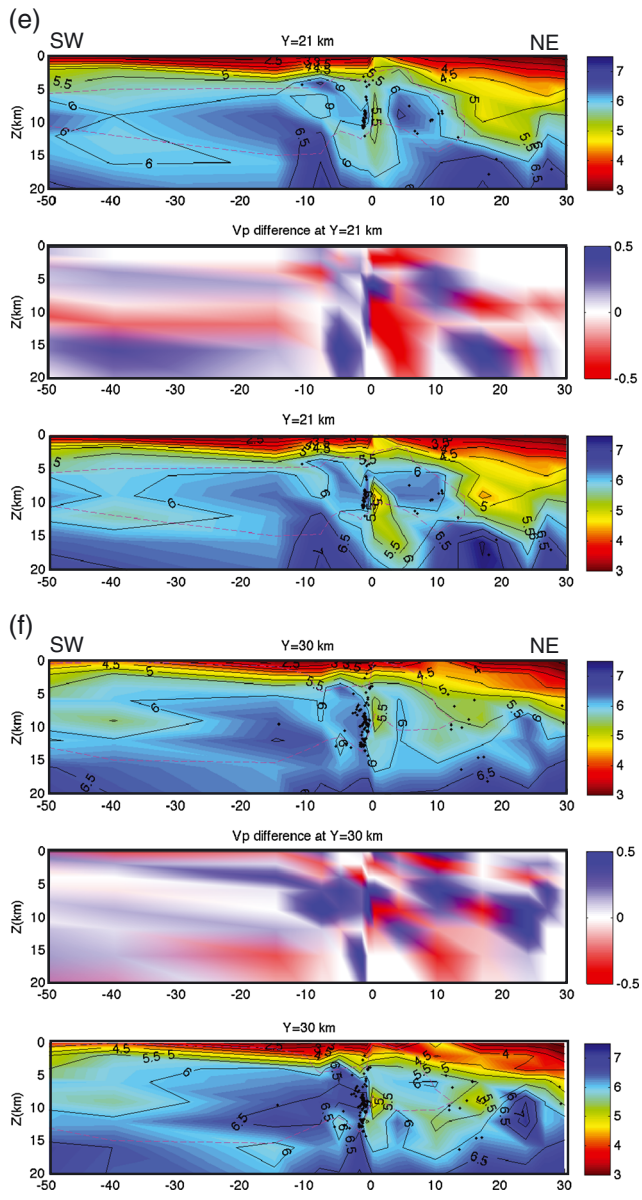

Figure 3. (Continued).

calculated based on each ray's distance to a particular grid node [*Toomey and Foulger*, 1989]. The derivative weight sum value of 200 corresponds to areas in the recovered synthetic model that are well recovered under checkerboard tests (E-supp Text C and Figure C1). Dashed magenta lines in Figure 3 and E-supp Figure B1 represent well-resolved regions of the model (derivative weight sum values > 200).

[11] The inclusion of the DWSA times increases the overall number and density of ray paths sampling the fault zone. The resulting Vp model shows an increase in the across-fault velocity contrast relative to the starting model (Figure 3). Overall, contours of high and low velocity on opposing sides of the fault move to align nearer to and/or along zones of seismicity, yielding an overall increase in the across-fault velocity contrast. Cross sections NW of the 1966 Parkfield earthquake hypocenter (Figures 3a and 3b: Y = −21 and −15 km; Z = 3 to 10 km) show the 5.5 and 6 km/s contours moving to align nearer to and along the seismicity. The >6 km/s values seen here on the SW side of the seismicity are representative of the high Vp rocks of the Salinian block [*Thurber et al.*, 2006]. Vp values decrease to as low as 3 to 4 km/s moving NE of the seismicity, likely representing the Franciscan and Great Valley sequences. Between the 1966 and 2004 Parkfield earthquake hypocenters (Figures 3c and 3d: Y = 3 and 6 km; Z = 5 to 15 km), Vp values SW of the seismicity slightly decrease to 6.0 km/s and values NE of the seismicity increase to near ~6.6 km/s with a maximum value of 7.3 km/s. This yields a reversal in the across-fault velocity contrast relative to that seen NW of the 1966 hypocenter. In this case, we have fast materials on both sides of the fault with the faster material lying NE of the seismicity. Figures 3c and 3d show that the faster material, lying NE of the seismicity, is ~2 km thick in the X-direction, and Figure 4 shows the across-fault reversal in velocity contrast extending from Y = 0 to 15 km. Checkerboard tests

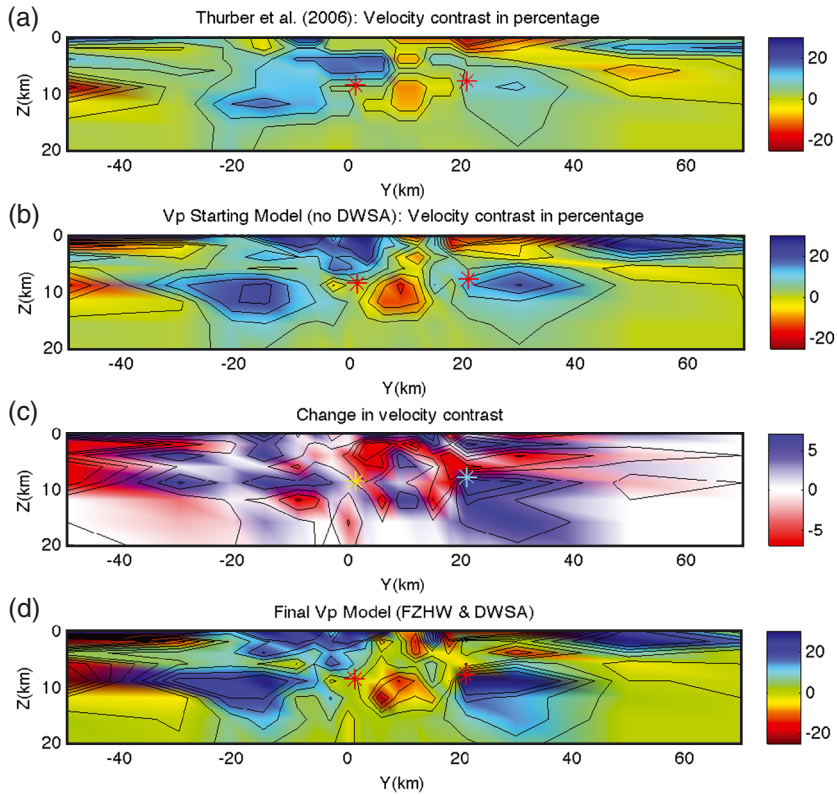

Figure 4. (a) The across-fault velocity contrast for the Vp model of *Thurber et al*. (2006). (b) The starting model velocity contrast across the fault where DWSA data are excluded. (c) Perturbations to the starting model when DWSA data are incorporated. (d) The across-fault velocity contrast for the Vp model where DWSA data are incorporated. Left and right stars indicate the 1966 and 2004 Parkfield earthquake hypocenters, respectively. The across-fault velocity contrast is calculated by differencing nodes immediately adjacent to seismicity, cross sections X = −1.75 km minus X = 0.25 km.

(E-supp Figure B1) demonstrate that a feature of this thickness, extending from Y = 0 to 15 km, is well recovered for Z ≤ 12 km, indicating that the higher velocity feature and obtained reversal in the across-fault velocity contrast are real.

[12] *Ebherhart-Phillips and Michaels* [1993] and *Thurber et al*. [2006] noted this reversal with *Thurber et al*. [2006] observing a maximum value of 6.6 km/s for Vp on the NE side of the seismicity. Vp values observed NE of the seismicity in this study and *Thurber et al*. [2006] are too high to be associated with the Salinian block. *Thurber et al*. [2006] suggested that this fast region is associated with the high-Vp greenstone and mafic rocks of the Permanente Terrane. *Brocher* [2008] estimated a Vp of ~6.9 km/s and ~6.7 km/s for mafic and greenstone rocks of northern California, which fits well with values observed in our study.

[13] Near and to the SE of the 2004 hypocenter (Figures 3e and 3f: Y = 18 and 30 km; Z = 5 to 12 km), the velocity contrast reverts back to the pattern seen NW of the 1966 hypocenter, where Vp values SW of the seismicity are higher than those to the NE. Again, we see the 6 km/s contour on the SW side of the seismicity moving to align along the seismicity, with maximum Vp values of 6.4 km/s immediately SW of the seismicity. In approximately the same region, *Thurber et al*. [2006] showed a maximum Vp of ~6 km/s. NE of the seismicity, the high-velocity body previously observed at Y = 6 km has migrated further NE and an area of lower Vp (5.5 to 6 km/s) separates it from the seismicity, as also seen in *Thurber et al*. [2006].

[14] The location of seismicity near the SAF trace suggests that the active fault surface falls near X = −0.75 km. To quantify the across-fault velocity contrast, the difference is taken between Vp model values immediately SW (at X = −1.75 km) and NE (at X = 0.25 km) of the seismicity. Figures 4a, 4b, and 4d show the across-fault velocity contrast of *Thurber et al*. [2006], the starting Vp model used in this study, and the final Vp model with DWSA times included, respectively. The across-fault velocity contrast seen in our starting model differs from that in *Thurber et al*. [2006] by as much as 5% due to the inclusion of FZHW's. For the central portion of the starting model (Y = −6 to 12 km), incorporation of *Zhang et al*.'*s* [2009] data set and finer gridding in the general area of that study region also influences the recovered starting model. We observe that inclusion of DWSA data increases the amplitude of the across-fault velocity contrasts (both negative and positive) by as much as 5% relative to the starting model and as much as 10% relative to that of *Thurber et al*. [2006]. Additionally, the DWSA-constrained Vp model produces velocity contrast regions that extend farther along the fault than the same regions seen in the starting model (Figure 4b) or that of *Thurber et al*. [2006] (Figure 4a).

[15] For the three models shown in Figure 4, we observe a positive velocity contrast NW of the 1966 hypocenter, a

striking negative velocity contrast between the hypocenters of the 1966 and 2004 Parkfield earthquakes, and a positive across-fault velocity contrast to the SE of the 2004 hypocenter. Figure 4d shows the positive velocity contrast NW of the 1966 hypocenter to be an elongate feature extending from immediately NW of the 1966 hypocenter nearly to Y = −40 km and having values as large as 20%. *Zhao et al*. [2010] used moveout curves between first-arriving FZHW and later-arriving DWSA to estimate the across-fault velocity contrast in this region and find a maximum value of ~20%, which agrees well with our results.

[16] Adjacent to this region, the strong negative velocity contrast (as high as −18%) existing from Z = 7 to 15 km depth and Y = −2 to 15 km demarcates the negative velocity contrast region. Due to the spatial distribution of stations and local seismicity, *Zhao et al*. [2010] had difficulty resolving the value of a negative velocity contrast in this region. *Thurber et al*. [2006] noted a possible spatial relationship between this region and the coseismic slip associated with the 2004 Parkfield earthquake.

[17] We compare a suite of coseismic slip models for the 2004 Parkfield earthquake determined via geodetic and/or strong motion data [*Kim and Dreger*, 2008; *Custódio et al*., 2009; *Barnhart and Lohman*, 2010; *Bennington et al*., 2011] to the negative velocity contrast area. Contours of peak coseismic slip (≥0.3 m) are overlain on the Vp contrast determined in this study (Figure 5). A strong correlation is observed between the lateral extent of the main slip patch of the slip models and the negative velocity contrast seen in our model, although the depth ranges differ: peak slip in three of these coseismic slip models extends from 5 to 10 km depth while the main negative velocity contrast exists from 7 to 15 km. Interestingly, the main patches of peak slip seen in the coseismic slip model of *Kim and Dreger* [2008] (Figure 5, white dashed line) are located within the extents of the main negative velocity contrast and a smaller negative velocity contrast centered at Y = 22 km and Z = 12 km. This suggests that the negative velocity contrast observed here played a part in defining the rupture patch for the 2004 Parkfield earthquake.

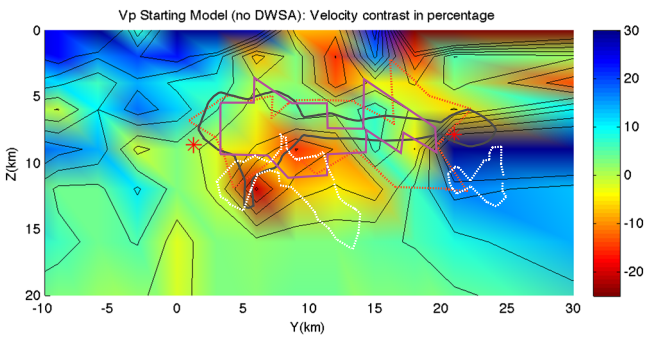

Figure 5. Vp model incorporating first-arriving P wave and FZHWs and DWSAs is shown as colored model. Overlain solid grey, dashed white, solid magenta, and dashed red lines represent the >0.3 m slip contour of the coseismic slip models of *Custódio et al*. [2009], *Kim and Dreger* [2008], *Bennington et al*. [2011], and *Barnhart and Lohman* [2010], respectively.

[18] SE of the 2004 hypocenter, *Zhao et al*. [2010] observed a sparseness of FZHWs and infer an absent or very small velocity contrast. For the same region, we observe a velocity contrast at Z ≤ 3 km of −15 to −5% and, immediately below this, a positive velocity contrast of 5 to 15% at Z = 5 to 12 km. *Zhao et al*. [2010] suggested that the propagation of FZHWs through regions of varied velocity contrasts could reduce the velocity contrast values they obtained. Thus, the juxtaposition of the high negative and high positive velocity contrasts in this region could yield a lack of observable FZHW's.

[19] *Harris and Day* [2005] examined M6 earthquakes that occurred in Parkfield in 1934, 1966, and 2004 together with several M4 and M5 earthquakes. Through numerical simulations, they suggest that the bimaterial interface is an unlikely predictor of rupture propagation direction. *Ben*-Zion [2006] argued that the eight M4–M6 Parkfield earthquakes examined by *Harris and* Day [2005] were small to moderate, suggesting that the events could be controlled by local structural complexities. Additionally, the total number of events examined is not statistically significant. Nevertheless, if we assume that rupture direction is controlled by the bimaterial interface [*Ampuero and Ben-Zion*, 2008], we can use the velocity contrasts in Figure 4 for "prediction" of the preferred rupture propagation directions of the 1966 and 2004 Parkfield earthquakes. The 2004 Parkfield earthquake is located between a large, positive velocity contrast to the SE and a large, negative velocity contrast to the NW. Following *Ampuero and Ben-Zion* [2008], the positive velocity contrast suggests a preferred propagation direction to the SE, whereas the negative velocity contrast suggests a preferred propagation direction to the NW. Taken together, this suggests bilateral rupture propagation as was observed during the 2004 Parkfield earthquake. The velocity contrasts abutting the 1966 Parkfield earthquake would suggest bilateral rupture in a similar manner. However, the velocity-strengthening behavior of the creeping section of the SAF would prevent rupture to the NW. Thus, it is not surprising that rupture propagated only to the SE during this event.

[20] Finally, we note that *Zhao et al*. [2010] picked FZHWs and DWSA's based only on their waveform characteristics (emergent vs. sharp) and opposite polarities. The method of *Bulut et al*. [2012] used an additional constraint based on differences in the polarizations of FZHWs and DWSAs and would, therefore, result in more reliable phase picks. Our imaging resolution could be improved further by using more accurate picks through the method of *Bulut et al*. [2012] and/or other methods. This is beyond the scope of this paper and will be pursued in subsequent studies.

5. Conclusion

[21] We incorporate a set of FZHW and DWSA times into the existing set of first-arrival time data for the Parkfield region. We compare our final Vp model to that of *Thurber et al*. [2006] and find that the main features of the two models agree well. However, contours of high and low velocity on opposing sides of the fault move closer to the fault and align nearer to and/or along zones of seismicity, yielding an overall increase in the across-fault velocity

contrast relative to both our starting model and that of *Thurber et al*. [2006]. Looking along strike, three pronounced velocity contrast regions are observed: strong positive velocity contrasts both NW of the 1966 Parkfield earthquake and SE of the 2004 Parkfield earthquake and a strong negative velocity contrast between the 1966 and 2004 events. Similar velocity contrasts were imaged by *Thurber et al*. [2006]. However, the inclusion of FZHW and DWSA data increases the size and amplitude of the across-fault velocity contrasts (both negative and positive), the latter by as much as 5% relative to our starting model and as much as 10% relative to that of *Thurber et al*. [2006]. We find that the area of the strong negative velocity contrast in our model agrees well with the lateral extent of peak coseismic slip estimated from both geodetic and strong motion studies. Three of the coseismic slip models examined place main shock slip from 5 to 10 km depth, while our negative velocity contrast exists from 7 to 15 km. One coseismic slip model [*Kim and Dreger*, 2008] places the two main peak slip patches entirely within the main negative velocity contrast and a smaller negative velocity contrasts located to the SE. This suggests that the negative velocity contrast played a role in defining the rupture patch for the 2004 Parkfield earthquake. Velocity contrasts at the 2004 Parkfield earthquake hypocenter suggest bilateral rupture propagation as was observed during the event. Velocity contrasts at the 1966 Parkfield hypocenter also suggest bilateral rupture, but given the velocity-strengthening behavior of the creeping section of the SAF to the NW, it is not surprising that rupture propagated only to the SE during this event.

[22] **Acknowledgments.** We thank the two anonymous reviewers and the Associate Editor for their useful comments. This work is supported by the United States Geological Survey NEHRP grants G11AP20027 and G11AP20028.

References

Ampuero, J.-P., and Y. Ben-Zion (2008), Cracks, pulses and macroscopic asymmetry of dynamic rupture on a bimaterial interface with velocity-weakening friction, *Geophys. J. Int.*, doi: 10.1111/j.1365-246X.2008.03736.x.

Andrews, D. J., and Y. Ben-Zion (1997), Wrinkle-like slip pulse on a fault between different materials, *J. Geophys. Res.*, *102*, 553–571.

Barnhart, W., and R. Lohman (2010), Automated fault discretization for inversions for coseismic slip distributions, *J. Geophys. Res.*, *115*, B10419, doi:10.1029/2010JB007545, in press.

Bennington, N., C. Thurber, K. Feigl, and J. Murray-Moraleda (2011), Aftershock distribution as a constraint on the geodetic model of coseismic slip for the 2004 Parkfield earthquake, *Pur. App. Geophys.*, *168*, 1553–1565.

Ben-Zion, Y. (1989), The response of two joined quarter spaces to SH line sources located at the material discontinuity interface, *Geophys. J. Int.*, *98*, 213–222.

Ben-Zion, Y. (1990), The response of two half spaces to point dislocations at the material interface, *Geophys. J. Int.*, *101*, 507–528.

Ben-Zion, Y. (2006), Comment on "Material contrast does not predict earthquake rupture propagation direction" by R. A. Harris and S. M. Day, *Geophys. Res. Letters*, *33*, L13310.

Ben-Zion, Y., and K. Aki (1990), Seismic radiation from an SH line source in a laterally heterogeneous planar fault zone, *Bull. Seism. Soc. Am.*, *80*, 971–994.

Ben-Zion, Y., and P. Malin (1991), San Andreas fault zone head waves near Parkfield, *California, Science*, *251*, 1592–1594.

Ben-Zion, Y., S. Katz, and P. Leary (1992), Joint inversion of fault zone head waves and direct P arrivals for crustal structure near major faults, *J. Geophys. Res.*, *97*, 1943–1951.

Brocher, T. (2008), Compressional and shear-wave velocity versus depth relations for common rock types in northern California, *Bull. Seism. Soc. Am.*, *98*, 950–968.

Bulut, F., Y. Ben-Zion, and M. Bohnhoff (2012), Evidence for a bimaterial interface along the Mudurnu segment of the North Anatolian Fault Zone from polarization analysis of P waves, *Earth Planet. Sci. Lett.*, *327*, 17–22.

Custódio, S., M. Page, and R. Archuleta (2009), Constraining earthquake source inversions with GPS data: 2. A two-step approach to combine seismic and geodetic data sets, *J. Geophys. Res.*, *114*, B01315.

Eberhart-Phillips, D., and A. J. Michael (1993), Three-dimensional velocity structure, seismicity, and fault structure in the Parkfield region, central California, *J. Geophys. Res.*, *98*, 15,737–15,758.

Haslinger, F., and E. Kissling (2001), Investigating the effect of the applied ray tracing in local earthquake tomography, *Phys. Earth Plan Int.*, *123*, 103–114.

Harris, R., and S. Day (2005), Material contrast does not predict earthquake rupture propagation direction, *Geophys. Res. Letters*, *32*, doi: 10.1029/2005GL023941.

Kim, A., and D. Dreger (2008), Rupture process of the 2004 Parkfield earthquake from near-fault seismic waveform and geodetic records, *J. Geophys. Res.*, *113*, B07308.

Legliné, O., and J. Got (2011), Rupture directivity of microearthquake sequences near Parkfield, California, *Geophys. Res. Letters*, *38*, L08310, doi: 10.1029/2011GL047303.

Lewis, M. A., Y. Ben-Zion, and J. McGuire (2007), Imaging the deep structure of the San Andreas Fault south of Hollister with joint analysis of fault-zone head and direct P arrivals, *Geophys. J. Int.*, *169*, 1028–1042, doi: 10.1111/j.1365-246X.2006.03319.x.

McGuire, J., and Y. Ben-Zion (2005), High-resolution imaging of the Bear Valley section of the San Andreas fault at seismogenic depths with fault-zone head waves and relocated seismicity, *Geophys. J. Int.*, *163*, 152–164.

McLaughlin, R. J., W. V. Sliter, D. H. Sorg, P. C. Russell, and A. M. Sarna-Wojcicki (1996), Large-scale right-slip displacement on the east San Francisco Bay region fault system, California: Implications for location of late Miocene to Pliocene Pacific plate boundary, *Tectonics.*, *15*, 1-18.

Thurber, C., H. Zhang, F. Waldhauser, J. Hardebeck, A. Michael, and D. Eberhart-Phillips (2006), Three-dimensional compressional wavespeed model, earthquake relocations, and focal mechanisms for the Parkfield, California, region, *Bull. Seismol. Soc. Am.*, *96*, S38–S49.

Toomey, D., and G. Foulger (1989), Tomographic inversion of local earthquake data from the Hengill-Grensdalur central volcano complex, Iceland, *J. Geophys. Res.*, *94*, 17497–17510.

Um, J., and C. Thurber (1987), A fast algorithm for two-point seismic ray tracing, *Bull. Seism. Soc. Am.*, *77*, 972–986.

Zhang, H., and C. Thurber (2003), Double-difference tomography: The method and its application to the Hayward Fault, California, *Bull. Seismol. Soc. Am.*, *93*(5), 1875–1889; DOI: 10.1785/0120020190.

Zhang, H., C. Thurber, and P. Bedrosian (2009), Joint inversion for Vp, Vs, and Vp/Vs at SAFOD, Parkfield, California, *Geochem. Geophys. Geosyst.*, *10*, Q11002, doi:10.1029/2009GC002709.

Zhao, P., and Z. Peng (2008), Velocity contrast along the Calaveras fault from analysis of fault zone head waves generated by repeating earthquakes, *Geophys. Res. Lett.*, *35*, L01303, doi:10.1029/2007GL031810.

Zhao, P., Z. Peng, Z. Shi, M. Lewis, and Y. Ben-Zion (2010), Variations of the velocity contrast and rupture properties of M6 earthquakes along the Parkfield section of the San Andreas fault, *Geophys. J. Int.*, *180*, 765–780, 10.1111/j.1365-246X.2009.04436.x.